International Journal of Oceans and Oceanography
ISSN 0973-2667 Volume 1, Number 2 (2006), pp. 221-239
© Research India Publications
http://www.ripublication.com

A Three-Dimensional Numerical Model for Wave-Induced Transient Pore Pressure around the Head of a Breakwater

Dong-Sheng Jeng* and Jian Li

School of Civil Engineering, The University of Sydney, New South Wales 2006, Australia.

**Corresponding author: Email: d.jeng@civil.usyd.edu.au*

Abstract

The wave-induced pore pressure in marine sediment around a coastal structure has been recognised as a dominant factor in analysing the seabed instability in the vicinity of a breakwater. Most previous investigations for wave-induced pore water pressure have been limited to two-dimensions, which are not able to simulate the phenomenon around the head of a breakwater. In this paper, a three-dimensional numerical model for the wave-induced pore pressure around the head of a breakwater is established. With the present model, a parametric study is performed to investigate the effects of wave and soil characteristics on the seabed response. Numerical results conclude: (1) diffracted wave components significantly affect the distribution of pore water pressure, vertical effective normal stresses and liquefaction potential; (2) a liquefied hole occurs near the head of a breakwater; (3) incident wave angles do not only affect the pattern of liquefied regions, but also the maximum liquefaction depth; and (4) the soil type significantly affects the distribution of soil response and liquefaction, and liquefaction only occurs in fine sand, not coarse sand.

Keywords: pore pressure, vertical effective normal stresses, marine sediment, breakwater, liquefaction.

INTRODUCTION

Protection of the coastal environment is vital for countries like Australia, where more than 80% of total population is concentrated in coastal regions. Marine structures such as breakwaters are commonly adopted for such protection. Design of marine structures considering their stability is a rather complicated problem. One of important factors which have to be taken into consideration in the design procedure is the wave-induced seabed instability (liquefaction) in the vicinity of the structures. It

has been well documented that ocean waves propagating over the ocean surface exert dynamic pressure fluctuations on the sea floor. These fluctuations generate an excess pore pressure within the soil skeleton, which have been recognized as a dominant factor in analysing the seabed instability. Recently, numerous marine structures have been reported to be damaged by seabed instability at their toes [1]. Furthermore, it has been observed that a deep hole exists near the tip of a marine structure [2]. Without proper maintenance at these sites, failure of structures may be expected.

In general, the wave phenomenon in the vicinity of a marine structure contains two types of wave system, occurring in front of and at the tip of the structure (Figure 1). When waves arrive obliquely at a marine structure (zone A), portions of the crests are reflected from the wall. In this region, the incident waves will interact with their reflected waves, resulting in a short-crested wave system propagating along the breakwater. When the waves arrive at the tip of a marine structure in region B, the reflected waves are diffracted due to the discontinuity of the structure at the tip. Thus, the total wave is a combination of incident, reflected and diffracted waves. Because the reflected wave components do not exist in zone C, the wave system is a combination of incident and diffracted waves. Furthermore, only diffracted wave components exist in region D.

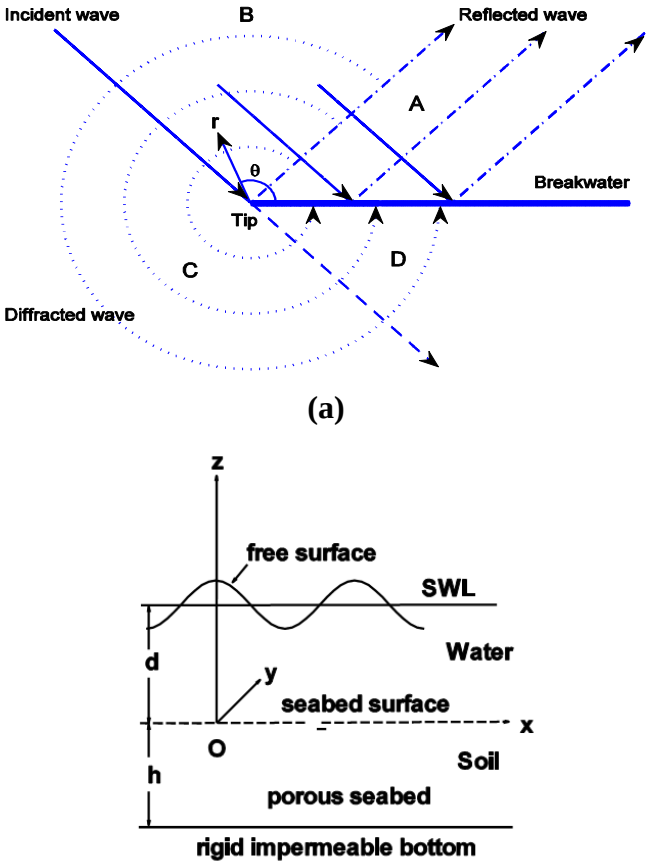

Figure 1: Sketch of wave-seabed interaction in the vicinity of a breakwater. (a) Wave field around a breakwater, and (b) Wave-seabed-structure interaction.

Numerous investigations for the wave-induced seabed response, including pore pressure, effective stresses and soil displacements, have been carried out since the 1970's. Among these, analytical approximations [3, 4], numerical modelling [5-7] and experimental work [8,9] have been adopted to investigate the wave-induced oscillatory pore pressure and momentary liquefaction in marine sediments. The contributions and limitation of previous studies in the area have been systematically reviewed in Jeng [10]. However, all previous models have been limited to either one-dimensional or two-dimensional cases, which can only represent part of the whole problem (i.e., Zone A in Figure 1)

Jeng [11] appears to be the unique study to investigate the wave-induced pore pressure and liquefaction at the tip of a breakwater. In his analytical model, only transient soil response in an infinite seabed was considered in the model. However, in reality seabeds are predominantly a porous medium of finite thickness. Therefore, the model cannot provide a complete understanding of the whole problem. In addition, a mistake is found in one of the governing equations used in his model, as mentioned in the next section. Thus, the results are doubtable, and it is desirable to establish a model with correct governing equations.

In addition to the seabed response due to ocean waves, the soil properties also affect the wave characteristics, especially the wave damping effects. According to Jeng [12], soil properties will appear in the wave dispersion relation, which has been used to determine the wavelength. Although wave damping affects the wave characteristics to a certain degree, its influence on the soil response is minor [12], to simplify the problem, we ignore the wave damping effects in this study.

In summary, the gaps between the previous investigations and proposed study are:

(a) Most previous investigations have only considered the wave-induced seabed response in front of a breakwater, rather than at the tip of a breakwater, although the latter is more important for engineering design.

(b) The existing studies for the wave-induced soil response at the tip of a breakwater only consider transient soil response in an infinite seabed with an incorrect governing equation. Thus, a better model for more realistic case of finite thickness is desired.

The major objective of this project is to investigate the wave-induced seabed response around the head of a breakwater. A numerical model will be established to implement the theory. In this paper, a finite difference model will be established. With the new numerical model, the influence of diffracted waves and other dominant factors on the wave-induced pore pressure will be examined. The potential of the wave-induced liquefaction will also be estimated.

Theoretical Formulations

Governing equations

The problem modelled in this study is depicted in Figure 1. With the assumptions of compressible pore fluid and soil and pore-elasticity, the wave-induced oscillating soil response is governed by Biot's consolidation equation [13], i.e.,

$$K\left(\frac{\partial^2 p}{\partial r^2}+\frac{1}{r}\frac{\partial p}{\partial r}+\frac{1}{r^2}\frac{\partial^2 p}{\partial \theta^2}+\frac{\partial^2 p}{\partial z^2}\right)-n_e\beta\gamma_w\frac{\partial p}{\partial t}=\gamma_w\frac{\partial \varepsilon}{\partial t} \tag{1}$$

where p is the wave-induced pore pressure, K, n_e, β and ε are soil permeability, soil porosity, compressibility of soil and volumetric strain, respectively. G is shear modulus, and μ is Poisson's ratio.

The compressibility of the soil (β) and the volumetric strain (ε) are defined by

$$\varepsilon=\varepsilon_r+\varepsilon_\theta+\varepsilon_z \quad \text{and} \quad \beta=\frac{1}{K'}+\frac{1-S}{P_{wo}} \tag{2}$$

in which ε_r, ε_θ and ε_z are the strain in the r-, θ- and z-directions defined in (4a)-(4c), respectively, $K'=2\times10^9$ N/m^2, S is the degree of saturation, and $P_{wo}=\gamma_w d$ (d is the water depth, γ_w is the unit weight of pore fluid).

Based on pore-elastic theory, the stress-strain relationship can be expressed as

$$\sigma'_r=2G\left(\varepsilon_r+\frac{\mu\varepsilon}{1-2\mu}\right), \tag{3a}$$

$$\sigma'_\theta=2G\left(\varepsilon_\theta+\frac{\mu\varepsilon}{1-2\mu}\right), \tag{3b}$$

$$\sigma'_z=2G\left(\varepsilon_z+\frac{\mu\varepsilon}{1-2\mu}\right), \tag{3c}$$

$$\tau_{r\theta}=2G\gamma_{r\theta}, \tag{3d}$$

$$\tau_{\theta z}=2G\gamma_{\theta z}, \tag{3e}$$

$$\tau_{rz}=2G\gamma_{rz}, \tag{3f}$$

where

$$\varepsilon_r=\frac{\partial u_r}{\partial r}, \qquad \varepsilon_\theta=\frac{u_r}{r}+\frac{1}{r}\frac{\partial u_\theta}{\partial \theta}, \qquad \varepsilon_z=\frac{\partial u_z}{\partial z}, \tag{4a}$$

$$\gamma_{r\theta}=\frac{1}{r}\frac{\partial u_r}{\partial \theta}+\frac{\partial u_\theta}{\partial r}-\frac{u_\theta}{r}, \tag{4b}$$

$$\gamma_{\theta z} = \frac{1}{r}\frac{\partial u_z}{\partial \theta} + \frac{\partial u_\theta}{\partial z}, \tag{4c}$$

$$\gamma_{rz} = \frac{\partial u_r}{\partial z} + \frac{\partial u_z}{\partial r}, \tag{4d}$$

The equations for force balance can be expressed as

$$\frac{1}{r}\frac{\partial (r\sigma'_r)}{\partial r} - \frac{\sigma'_\theta}{r} + \frac{1}{r}\frac{\partial \tau_{r\theta}}{\partial \theta} + \frac{\partial \tau_{rz}}{\partial z} = \frac{\partial p}{\partial r}, \tag{5a}$$

$$\frac{1}{r}\frac{\partial \sigma'_\theta}{\partial \theta} + \frac{\partial \tau_{\theta z}}{\partial z} + \frac{1}{r^2}\frac{\partial (r^2\tau_{r\theta})}{\partial r} = \frac{1}{r}\frac{\partial p}{\partial \theta}, \tag{5b}$$

$$\frac{\partial \sigma'_z}{\partial z} + \frac{1}{r}\frac{\partial (r\tau_{rz})}{\partial r} + \frac{1}{r}\frac{\partial \tau_{\theta z}}{\partial \theta} = \frac{\partial p}{\partial z}. \tag{5c}$$

Substituting (3a)-(3f) into (5a)-(5c), we have

$$2G\left\{\nabla^2 u_r + \frac{1-\mu}{1-2\mu}\frac{\partial \varepsilon}{\partial r} - \frac{1}{r}\frac{\partial}{r}\left(r\frac{\partial u_r}{\partial r}\right) - \frac{1}{r^2}\frac{\partial u_\theta}{\partial \theta}\right\} = \frac{\partial p}{\partial r}, \tag{6a}$$

$$2G\left\{\nabla^2 u_\theta + \frac{1}{r}\frac{1-\mu}{1-2\mu}\frac{\partial \varepsilon}{\partial \theta} + \frac{1}{r^2}\frac{\partial u_r}{\partial \theta} - \frac{u_\theta}{r^2} - \frac{1}{r^2}\frac{\partial^2 u_\theta}{\partial \theta^2}\right\} = \frac{1}{r}\frac{\partial p}{\partial \theta}, \tag{6b}$$

$$2G\left\{\nabla^2 u_z + \frac{1-\mu}{1-2\mu}\frac{\partial \varepsilon}{\partial z} - \frac{\partial^2 u_z}{\partial z^2}\right\} = \frac{\partial p}{\partial z}, \tag{6c}$$

It is noted that "1/*r*" on the right-hand-side of (6b) was missing in Jeng [11], which is corrected in this paper.

Boundary conditions

To solve the above governing equations, (1), (6a)-(6c), appropriate boundary conditions are required. First, the wave-induced pore pressure equals to dynamic wave pressure at the surface of the seabed, and vertical effective normal stress and shear stresses vanish, i.e.,

$$p = P_{b,} \quad \sigma'_z = \tau_{rz} = \tau_{\theta z} = 0 \quad \text{at} \quad z = 0 \tag{7}$$

where dynamic wave pressure at the surface of the seabed is given by [14],

$$P_b = p_0 \sum_{m=0}^{\infty} e^{-i\omega t} e^{-im\pi/4} \varepsilon_m J_{m/2}(kr)\cos\left(\frac{m\alpha}{2}\right)\cos\left(\frac{m\theta}{2}\right), \tag{8a}$$

$$p_0 = \frac{\gamma_w H_i}{2\cosh kd}, \qquad \varepsilon_m = \begin{Bmatrix} 1 & m = 0 \\ 2 & m \neq 0 \end{Bmatrix}, \tag{8b}$$

in which α is the incident wave angle, and $J_{m/2}$ is the first-kind of Bessel function with *m/2*-th order.

Second, the soil displacements and pressure gradient vanish at the seabed bottom, i.e.,

$$u_r = u_\theta = u_z = \frac{\partial p}{\partial z} = 0 \quad \text{at} \quad z = -h. \tag{9}$$

Third, assuming the breakwater is a rigid structure, impermeable boundary conditions are applied at both sides of walls, i.e.,

$$\frac{\partial p}{\partial n} = \sigma_n = 0 \quad \text{along} \quad \theta = 0,\ \theta = 2\pi \text{ and at r=0} \tag{10}$$

Finally, the boundary conditions at $r = L$ in zones A, B and C come from Jeng [4] and are taken as zeros in zone D.

Numerical scheme

In this study, we use the finite difference method to solve equations (1) and, (6a)-(6c) numerically. Suppose that all solutions are periodic and have the form $e^{-i\omega t}$ for the time *t*. The nodes and step sizes Δr, $\Delta\theta$ and Δz are defined by

$$\begin{aligned} &\Delta r = L/N, \quad \Delta\theta = 2\pi/M, \quad \Delta z = h/J, \\ &r_n = n\Delta r, \quad n = 0,\cdots,N, \\ &\theta_m = m\Delta\theta, \quad m = 0,\cdots,M, \\ &z_j = j\Delta z, \quad j = 0,\cdots,J, \end{aligned} \tag{11}$$

where *N*, *M* and *J* are the mesh in the *r*-, θ- and *z*-directions, respectively.

Let $p_m^{n,j}$ denote the value of *p* at the (r_n, θ_m, z_j)-th node. The finite difference scheme of equation (1) is constructed as follows

$$\frac{p_m^{n+1,j} - 2p_m^{n,j} + p_m^{n-1,j}}{\Delta r^2} + \frac{1}{r_n}\frac{p_m^{n+1,j} - p_m^{n-1,j}}{2\Delta r} + \frac{1}{r_n^2}\frac{p_{m+1}^{n,j} - 2p_m^{n,j} + p_{m-1}^{n,j}}{\Delta\theta^2}$$

$$+ \frac{p_m^{n,j+1} - 2p_m^{n,j} + p_m^{n,j-1}}{\Delta z^2} + \frac{in_e\beta\gamma_w\omega}{K}p_m^{n,j} = -\frac{i\gamma_w\omega}{K}\varepsilon_m^{n,j}. \tag{12}$$

The Neumann boundary conditions are approximated by the use of a second-order accurate formulae. Then we get the following equation

$$A_p p = f_p(u_r, u_\theta, u_z). \tag{13}$$

Similarly, (6a)-(6c) can be re-written as

$$A_{u_r} u_r = f_{u_r}(p, u_\theta, u_z). \tag{14a}$$

$$A_{u_\theta} u_\theta = f_{u_\theta}(p, u_r, u_z). \tag{14b}$$

$$A_{u_z} u_z = f_{u_z}(p, u_r, u_\theta). \tag{14c}$$

In the iterative procedure, successive over-relaxation (SOR) is first used to solve equations (13)-(14c) separately. We use ω_{SOR} ($0<\omega_{SOR}<2$) to denote the relaxation parameter, which may be different for each of the equations (13)-(14c). Second, under-relaxation is employed in order to obtain convergent solutions. Let ω_{UR} be the relaxation parameter and ε_c the criteria for the iterative procedure to converge. In our computations, we take $\varepsilon_c = 10^{-8}$. For example, we obtain $u_r^{(k+1)}$ as the iterative solution of equation (14a) if

$$\left| u_r^{(k+1)} - u_r^k \right| < \varepsilon_c, \tag{15}$$

and then the iterative procedure is terminated, otherwise the new ($k+1$)-th value which is introduced into the next iteration is given by

$$u_r^{(k+1)} = \omega_{UR} u_r^{(k+1)} + (1-\omega_{UR}) u_r^{(k)}, \tag{16}$$

where $0 < \omega_{UR} \le 1$.

RESULTS AND DISCUSSIONS

The effects of wave and soil characteristics on the wave-induced pore pressure and effective stresses in marine sediments have been discussed in the previous work with two-dimensional models [4]. Thus, the objectives of this paper are to examine the influence of factors, which only exist in three-dimensional cases, such as diffracted wave components and incident wave angles, on the wave-induced pore pressure and effective stresses around the head of a breakwater. The input data for numerical examples are tabulated in Table 1. In our numerical procedure we take $\omega_{SOR} = 1.4$ or 1, $\omega_{UR} = 0.01$, N=25, M=32 and J=20.

Table 1: Input data for numerical examples.

Wave characteristics	
Wave period (*T*)	12.0 sec
Water depth (*d*)	20 m
Wave length (*L*)	113.27 m
Wave height (*H*)	10 m
Soil characteristics	
seabed thickness (*h*)	25 m
Poisson's ratio (μ)	0.333
Soil porosity (n_e)	0.3
Shear modulus (*G*)	10^7 or 5×10^6 N/m^2
Soil permeability (*K*)	10^{-2}, 10^{-4} or 10^{-6} m/sec
Unit weight of soil (γ_s)	$2.65\gamma_w$
Unit weight of pore fluid (γ_w)	9806 N/m^3
Degree of saturation (*S*)	0.98
Coefficient of earth pressure (K_o)	0.5

Diffracted waves

The major differences between the present 3-D and previous 2-D models are the consideration of wave diffraction, which only occurs near the head of a breakwater. The contour distributions of the non-dimensional wave-induced pore pressure (p/p_0) at soil depth *z*=-1 m at different time intervals is illustrated in Figure 2. Since we focus on the region near the head of a breakwater, we only present the results within *r/L*=1. In the figure, the incident wave angle is 135 degrees ($\alpha = 3\pi/4$). As shown in the figure, the wave troughs move from the north-west (i.e., $\theta = 3\pi/4$) at *t/T*=0 (Figure 2(a)) to the head of a breakwater at *t/T*=1/2 (Figure 2(c)). It is noted that the magnitude of maximum pore pressure does not vary with time.

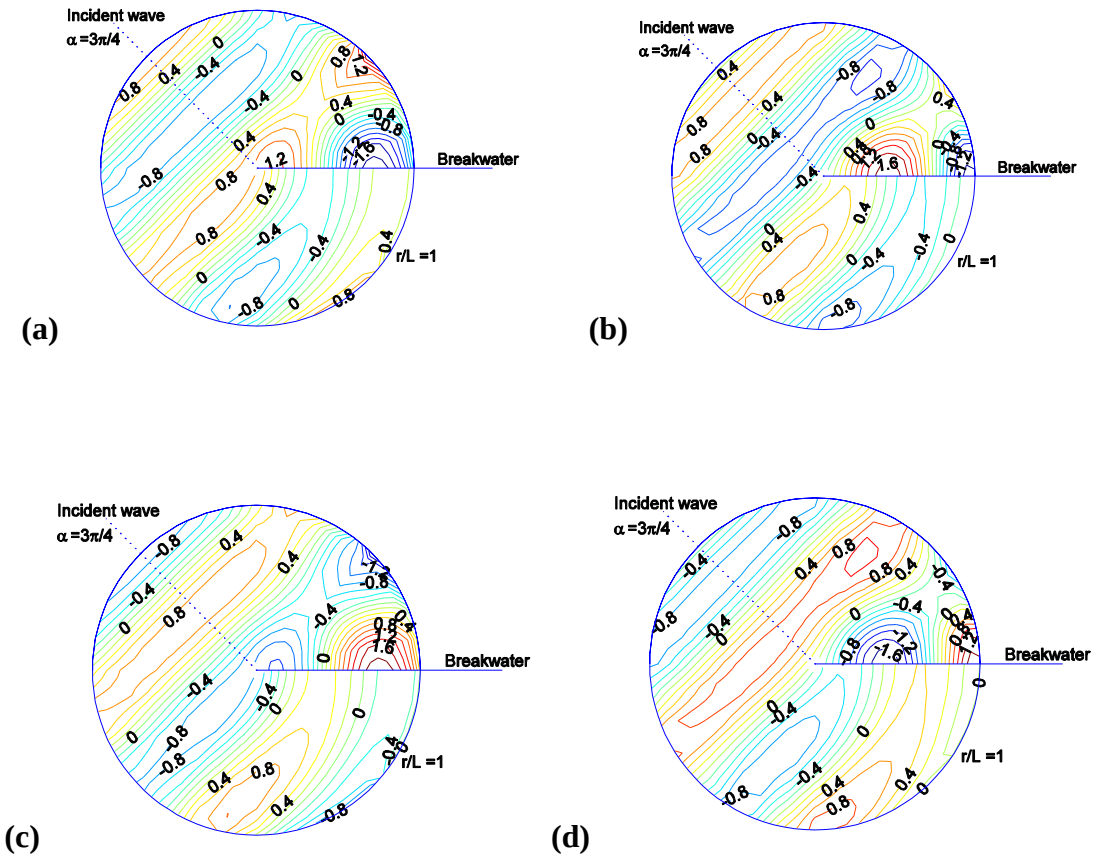

Figure 2: Contours of the wave-induced pore pressure (p / p_0) at *z*=-1 m for various time intervals. ($\alpha = 3\pi/4$, $K = 10^{-2}$ m/sec, $G = 10^7$ N/m^2). (a) *t*/*T*=0, (b) *t*/*T*=1/4, (c) *t*/*T*=1/2 and (d) *t*/*T*=3/4.

Figure 3 illustrates the contour distributions of the vertical effective normal stresses ($\sigma_z^{'} / p_0$) for various time intervals at *z*=-1 m. The figure indicates that the vertical effective normal stress ($\sigma_z^{'} / p_0$) has a phase difference of $\pi/2$ from the pore pressure, as shown in Figures 2 and 3. That is, a negative vertical effective normal stress occurs at the head of a breakwater when *t*/*T*=0, while it is positive when *t*/*T*=1/2.

Referring to Figure 1, Figures 2 and 3 demonstrate the significant effects of diffracted waves on the pore pressure distribution near the head of a breakwater, compared with that in front of a breakwater (i.e., Zone A in Figure 1).

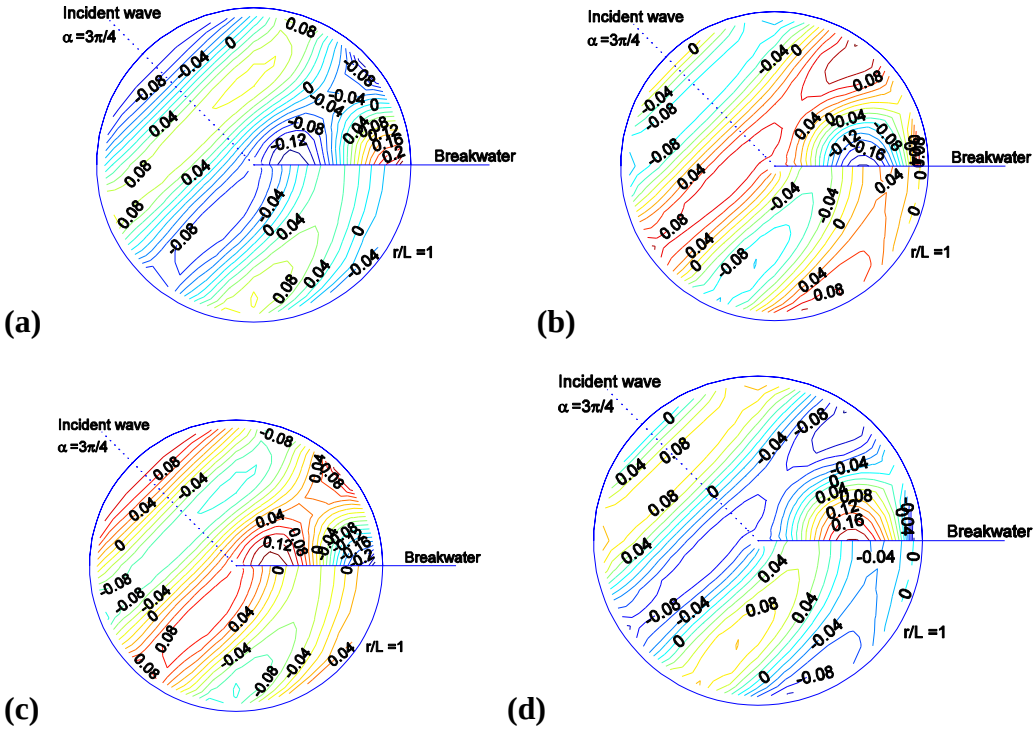

Figure 3: Contours of the wave-induced vertical effective normal stresses (σ_z' / p_0) at z=-1 m for various time intervals. ($\alpha = 3\pi/4$, $K = 10^{-2}$ m/sec, $G = 10^7$ N/m^2). (a) t/T=0, (b) t/T=1/4, (c) t/T=1/2 and (d) t/T=3/4.

Wave obliquity

The wave obliquity is another factor which only exists in three-dimensional cases. The vertical distributions of the wave-induced pore pressure (p / p_0) and vertical effective normal stress (σ_z' / p_0) versus relative soil depth (z/h) for various locations in radial direction (θ-direction) with different incident wave angles ($\alpha = \pi/4$, $\pi/2$, $3\pi/4$ and π) at r/L=0.1, t=0 are presented in Figures 4 and 5. In the figures, several locations in the θ-direction are chosen, i.e., $\theta = 0$, $\pi/4$, $\pi/2$, $3\pi/4$, π, $5\pi/4$, $3\pi/2$, $7\pi/4$ and 2π. In the case of $\alpha = \pi$ (Figures 4(d) and 5(d)), the lines for $\theta = 0$ and 2π ($\pi/4$ and $7\pi/4$, $\pi/2$ and $3\pi/2$, $3\pi/4$ and $5\pi/4$) are identical. As shown in the figure, the magnitude of the pore pressure and vertical effective normal stresses decrease as the θ increases, as the wave-induced pore pressure gradually decreases from the front of a breakwater to the rear of a breakwater. This trend is obvious at $\alpha = \pi/4$, and becomes less obvious as α increases.

Figures 6 and 7 show the transverse variations of p / p_0 and σ_z' / p_0 with $\alpha = \pi/4$, $\pi/2$, $3\pi/4$ and π for r/L=0.05, 0.1, 0.1, $\cdots$, 0.5 at $\theta = \pi/4$, t=0. The pore pressure and vertical effective normal stresses vary dramatically for $r/L \le 0.2$ and the depth of soil being between 0 and 12.5m.

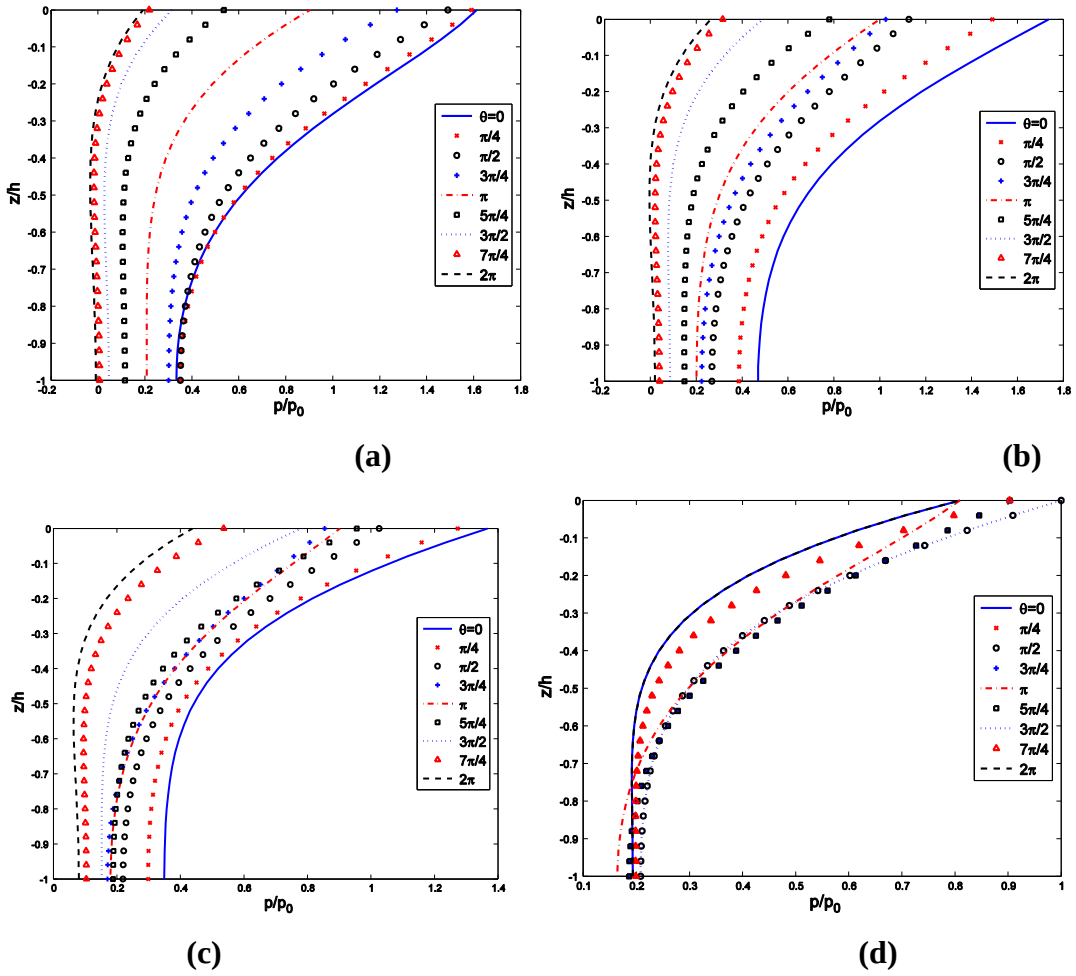

Figure 4: Vertical distributions of the wave-induced pore pressure (p / p_0) versus *z/h* for various values of θ. ($K = 10^{-2}$ m/sec, $G = 10^7$ N/m^2). (a) $\alpha = \pi / 4$, (b) $\alpha = \pi / 2$, (c) $\alpha = 3\pi / 4$ and (d) $\alpha = \pi$.

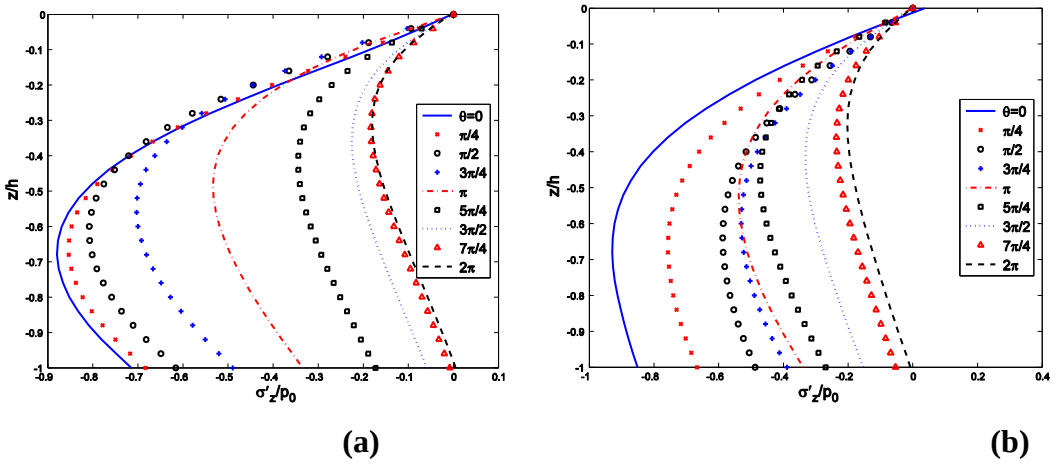

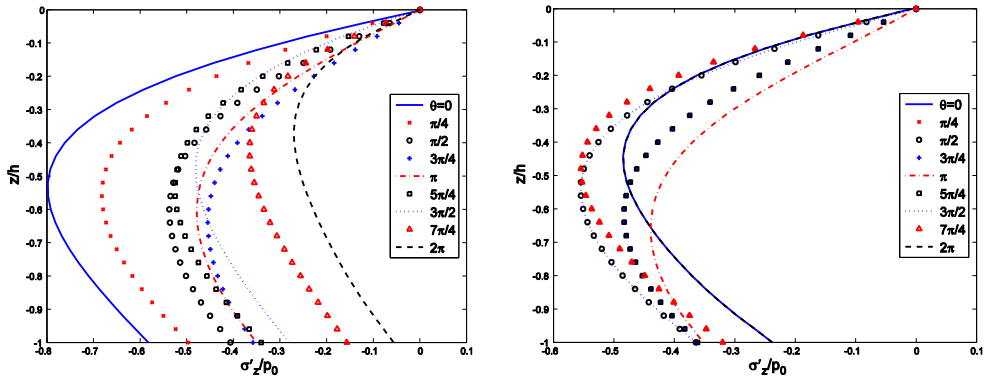

(c) **(d)**

Figure 5: Vertical distributions of the wave-induced vertical effective normal stresses ($\sigma_z^{'} / p_0$) for various values of θ. ($K = 10^{-2}$ m/sec, $G = 10^7$ N/m^2). (a) $\alpha = \pi/4$, (b) $\alpha = \pi/2$, (c) $\alpha = 3\pi/4$ and (d) $\alpha = \pi$.

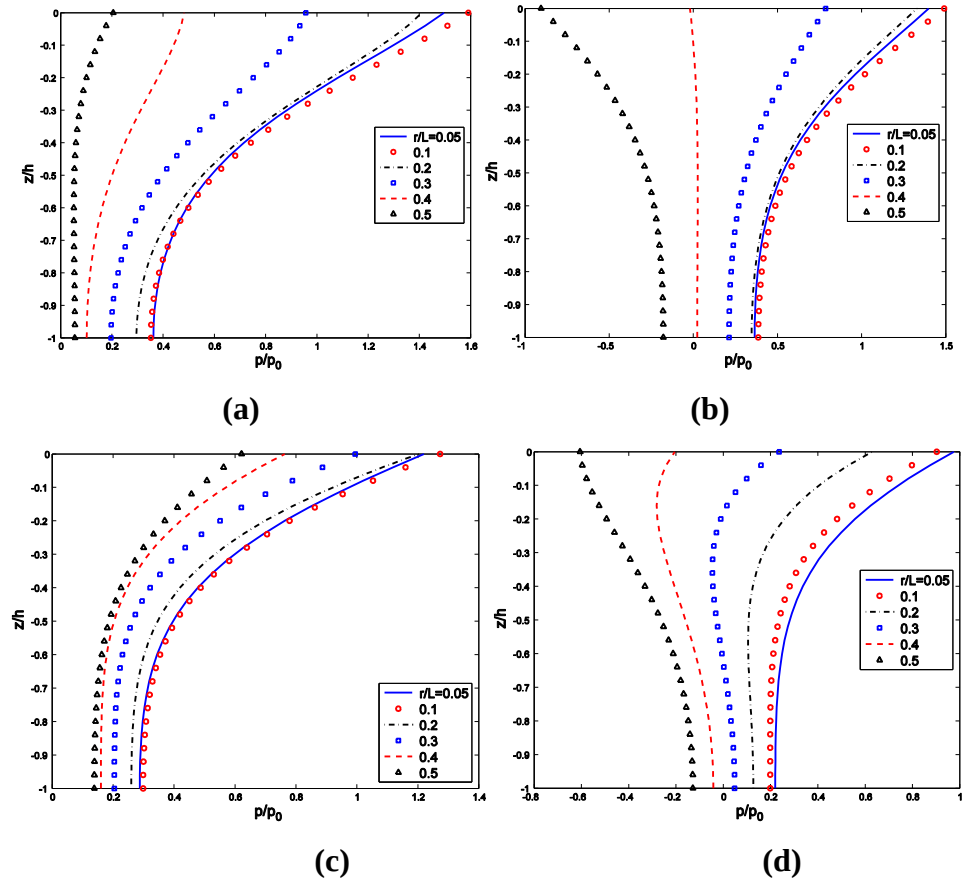

(a) **(b)**

(c) **(d)**

Figure 6: Vertical distributions of the wave-induced pore pressure (p / p_0) versus *z/h* for various values of *r/L*. ($K = 10^{-2}$ m/sec, $G = 10^7$ N/m^2). (a) $\alpha = \pi/4$, (b) $\alpha = \pi/2$, (c) $\alpha = 3\pi/4$ and (d) $\alpha = \pi$

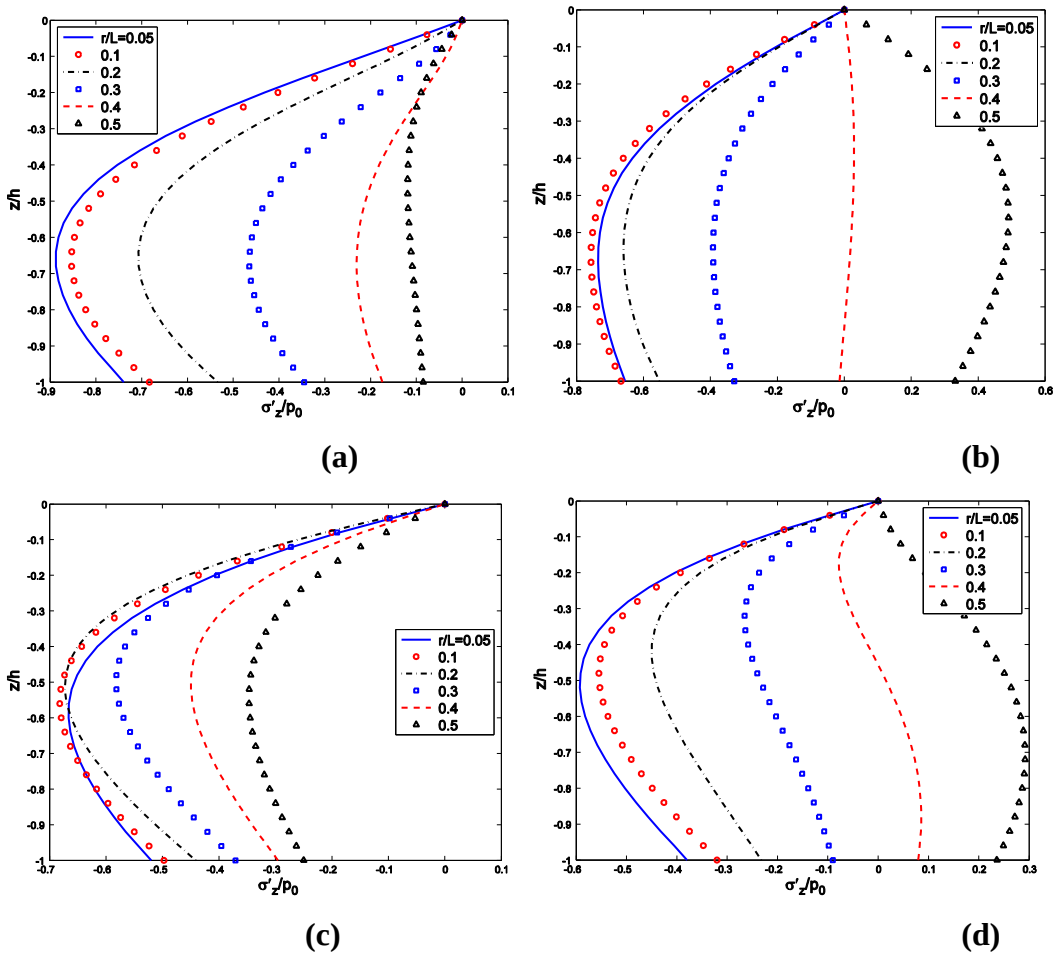

Figure 7: Vertical distributions of the wave-induced vertical effective normal stresses ($\sigma_z^{'} / p_0$) for various values of *r/L*. ($K = 10^{-2}$ m/sec, $G = 10^7$ N/m^2). (a) $\alpha = \pi / 4$, (b) $\alpha = \pi / 2$, (c) $\alpha = 3\pi / 4$ and (d) $\alpha = \pi$.

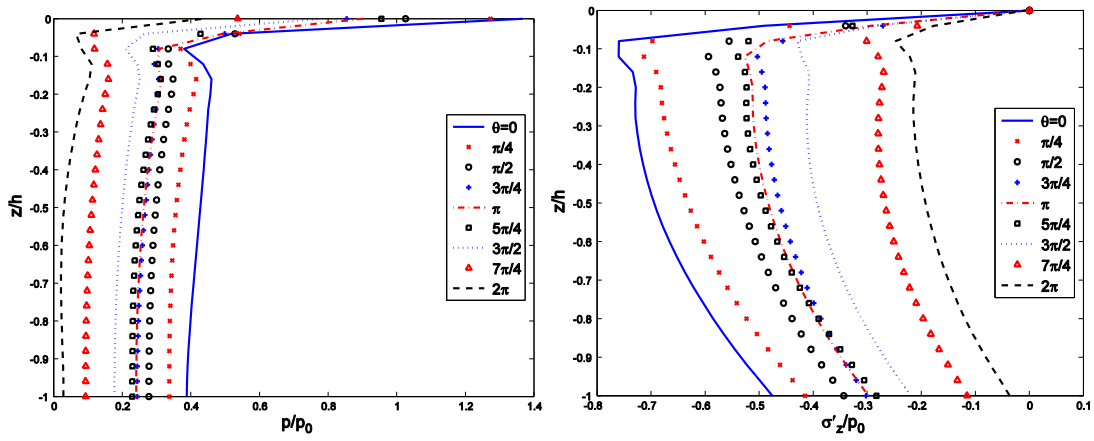

(A)

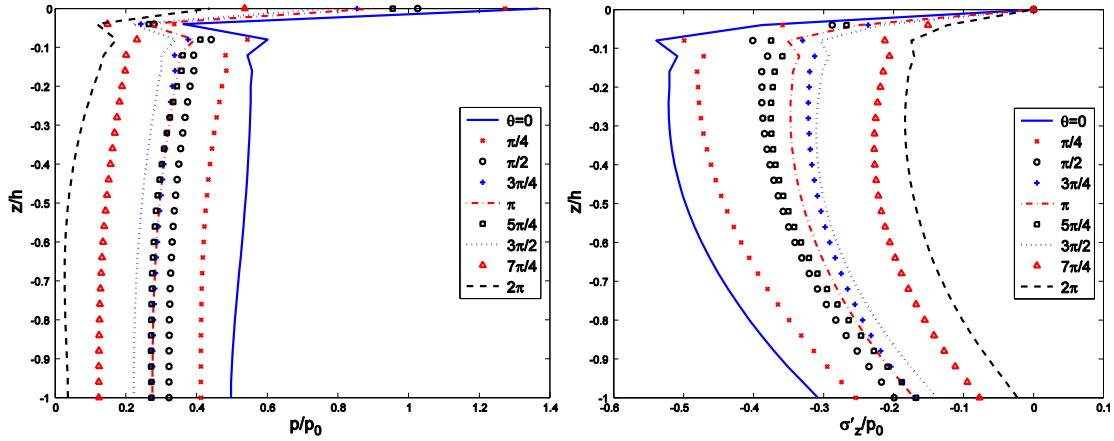

(B)

Figure 8: Vertical distributions of the wave-induced pore pressure (p/p_0) and vertical effective normal stresses ($\sigma_z^{'}/p_0$) versus *z/h* for various values of θ in different soils. ($\alpha = 3\pi/4$, *r/L*=0.1, *t*=0) (a) $K = 10^{-4}$ m/sec and $G = 10^7$ N/m^2 and (b) $K = 10^{-6}$ m/sec and $G = 5\times10^6$ N/m^2

oil types

Soil type is another important factor in the evaluation of the wave-induced pore pressure and effective stresses in marine sediments. The numerical examples presented in Figures 2-7 are only for the case of coarse sand with $K = 10^{-2}$ m/sec and $G = 10^7$ N/m^2. In this section, we considered another two types of soil, in which the soil properties are given in Table 1.

The vertical distributions of the wave-induced pore pressure and effective stress versus relative soil depth for fine sand are plotted in Figure 8. Together with Figures 4(c) and 5(c), a significant difference trend between coarse sand and fine sand is observed. Specifically, the pore pressure and effective normal stress vary with relative soil depth increasing gradually in coarse sand (see Figures 4(c) and 5(c)), while they change rapidly near the surface of the seabed in the case of fine sand. Due to the dramatic change of pore pressure distribution, the excess pore pressure will be greater than the self-weight of the soil, causing liquefaction. The potential of the wave-induced liquefaction will be discussed in next section.

Wave-induced liquefaction potential

Generally speaking, the wave-induced effective stresses and strains cause intergranular slip at grain to grain contacts, leading to volumetric compaction of loose marine sediments. The relaxation in the soil skeleton would transfer effective stresses to the pore water, thus giving rise to the increase of pore water pressure. Consequently, the corresponding reduction in effective stresses leads to a structural rebound in the soil skeleton to absorb the difference in volumetric change between the compaction due to grain slips and the reduction in pore water volume due to the increased pore pressure. In the extreme case, the excess pore pressure may increase until all the intergranular (effective) stresses have been eliminated from the system. In this state, no shear resistance of the soil skeleton can be expected, and liquefaction may occur.

The pore pressure change, $p(r,\theta,0,t)$, is equal to the wave pressure change at the seabed surface, $P_b(r,\theta,0,t)$. The difference represents an ``excess" component of the pore pressure in the deposit, which is termed *excess pore pressure*. Since the wave pressure at the seabed surface varies according to the propagation of waves, it implies that not only the pore pressure. $p(r,\theta,z,t)$, but also the wave pressure, $P_b(r,\theta,0,t)$, fluctuate periodically. Thus, the excess pore pressure can be determined by taking account of this variation of the wave pressure at the seabed surface, which is defined by [15]

$$u_e = -(P_b - p), \tag{17}$$

The first term on the right hand side of equation (17) represents the hydrostatic pressure (given by equation (8a)), and the second comes from the wave-induced pore pressure within soils. The excess pore pressure expressed by equation (17) is transient in nature, because u_e and p are oscillatory and periodic in real ocean environments. Consequently, the effective stress varies periodically in accordance with the change of the excess pore pressure. As shown in Figure 9, if it is attains zero or a negative value at certain depth below the seabed surface, the soil skeleton will become liquefied. Thus, the criterion of the wave-induced liquefaction can be expressed as

$$-\frac{1}{3}(\gamma_s - \gamma_w)(1+2K_0)z \le -(P_b - p), \tag{18}$$

where γ_s and γ_w are the unit weight of the soil and water, respectively. K_0 is the coefficient of lateral earth pressure at rest which varies from 0.4 to 1.0 in most soils. In equation (18), the left hand side represents the initial mean effective stress, while the right hand side denotes the excess pore pressure. It is important to note that the left hand side of equation (18) also represents the static stress field. To simplify the complicated problem, it is considered as uniform here, although it may be concentrated in the vicinity of the tip in the real case.

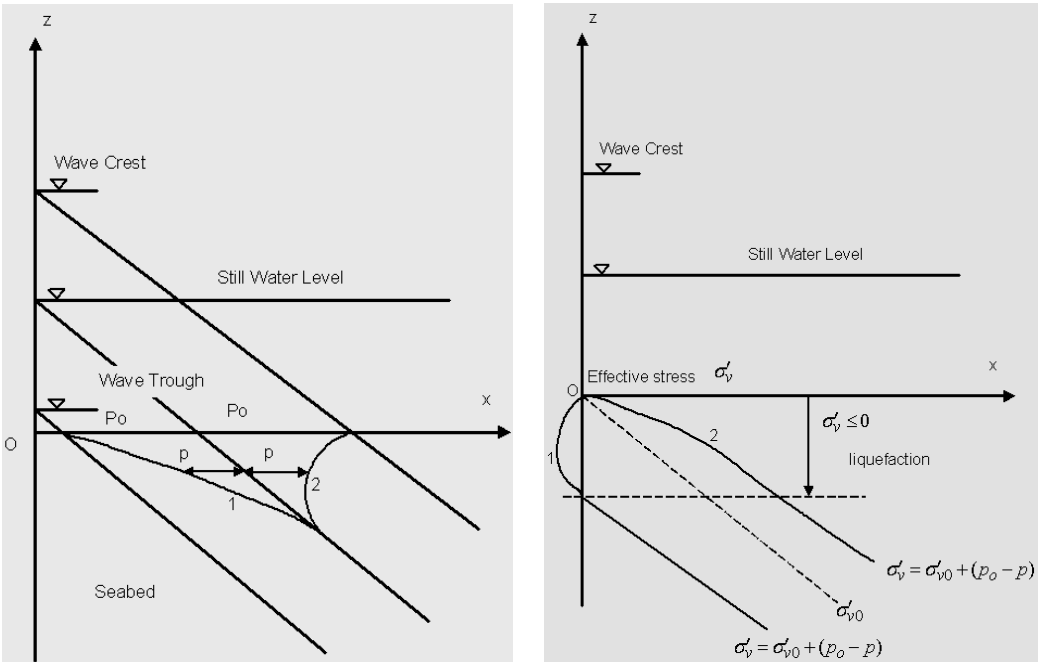

(A) **(B)**

Figure 9: Schematic sketch showing definition of liquefaction based on excess pore pressure. (After Zen and Yamamzaki [15]).

It has been reported that the wave induced liquefaction only occurs under the action of wave troughs [4, 14]. Thus, in this section, we only present the results at *t/T*=1/2, when the wave trough arrives the head of the breakwater, which is our main concern.

The wave-induced liquefaction potentials around the head of a breakwater for various incident wave angles are presented in Figure 10. As shown in the figure, the maximum liquefaction depth occurs near the head of a breakwater. This liquefied region forms a hole near the head of a breakwater, which raises more concerns on the design of the foundations of the structures. The incident wave angle does not only affect the pattern of liquefied regions, but also the magnitude of the maximum liquefaction depth near the head of a breakwater. For example, the maximum depth of the liquefied hole is about 3 m for $\alpha = \pi/4$, 4 m for with $\alpha = \pi/2$, 2.5 m for

$\alpha = 3\pi/4$, and 1.5 m for $\alpha = \pi$. It is noted that no liquefaction occurs in a seabed of coarse sand (graphs not shown).

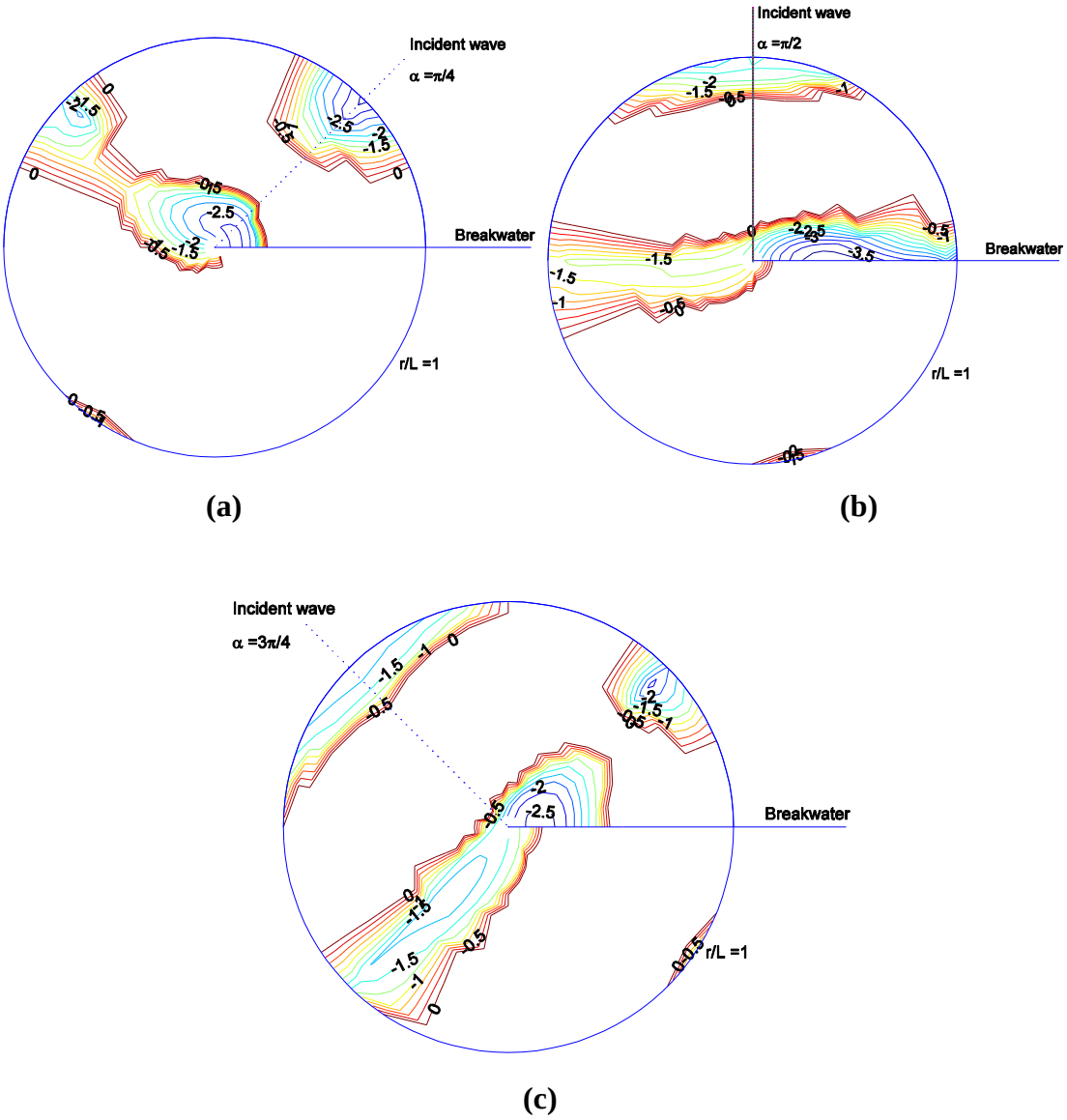

Figure 10: The wave-induced liquefaction potential in the vicinity of a breakwater. (a) $\alpha = \pi/4$, (b) $\alpha = \pi/2$ and (c) $\alpha = 3\pi/4$. ($K = 10^{-4}$ m/sec, $G = 10^{7}$ N/m^2) (a) $\alpha = \pi/4$, (b) $\alpha = \pi/2$ and (c) $\alpha = 3\pi/4$.

CONCLUSIONS

In this paper, we propose a three-dimensional numerical model for the wave-induced pore pressure and effective stress in a porous seabed around the head of a breakwater. Based on the numerical examples presented, the following conclusions can be drawn:

(1) The components of wave diffraction are considered in the new model, and significantly affect the distribution of the wave-induced pore pressure and effective stresses, and liquefaction potential in the vicinity of a breakwater.

(2) As the numerical calculations indicated, the incident wave angle α directly influences both the magnitude and the distribution of the wave-induced liquefaction potential around the head of a breakwater. This comes from the consideration of diffracted wave components.

(3) Three different seabeds are considered in the numerical examples. It is found that soil type significantly affects the pore pressure and effective normal stresses. Also, there is no liquefaction in coarse sand.

ACKNOWLEDGEMENT

The authors are grateful for the financial support from USyd Research & Development Grant Scheme (2005).

REFERENCES

[1] Silvester, R. and Hsu, J. R. C. 1989. "Sine Revisited", Journal of Waterways, Port, Coastal and Ocean Engineering, A.S.C.E., **115**, pp. 327-344.

[2] Sumer, B. M. and Fredsoe, J. 2002. The Mechanics of Scour in the Marine Environment. World Scientific, 536pp.

[3] Madsen, O. S. 1978. "Wave-induced pore pressures and effective stresses in a porous bed", Geotechnique, **28**, pp. 377-393.

[4] Jeng, D.-S. 1997. Wave-Induced Seabed Response in Front of a Breakwater. PhD thesis, The University of Western Australia.

[5] Jeng, D.-S. 2003. "A general finite element model for wave-seabed-structure interaction", In: Numerical Analysis and Modelling in Geomechanics (edited by John Bull), E&N SPON, London, 51-100.

[6] Thomas, S. D. 1989. "A finite element model for the analysis of wave induced stresses, displacements and pore pressures in an unsaturated seabed. I. Theory", Computes and Geotechnics, **8**, pp.1-38.

[7] Thomas, S. D. 1995. "A finite element model for the analysis of wave induced stresses, displacements and pore pressures in an unsaturated seabed. II. Model verification", Computes and Geotechnics, **15**, pp.107-132.

[8] Tsui Y. T. and Helfrich, S. C. 1983. "Wave-induced pore pressures in submerged sand layer", Journal of Geotechnical Engineering, A.S.C.E., **109**, pp. 603-618.

[9] Tsai, C. P. 1995. "Wave-induced liquefaction potential in a porous seabed in front of a breakwater", Ocean Engineering, **22**, pp.1-18.

[10] Jeng, D.-S. 2003. "Wave-induced seafloor dynamics", Applied Mechanics Review, **56**(4), pp. 407-429.

[11] Jeng, D.-S. 1996. "Wave-induced liquefaction potential at the tip of a breakwater", Applied Ocean Research, **18**(5), pp. 229-241.

[12] Jeng, D.-S. 2001. "A new wave dispersion equation: Effects of soil characteristics", International Journal of Offshore Mechanics and Arctic Engineering, ASME, **125**(4), pp. 177-181.

[13] Biot, M. A. 1941. "General theory of three-dimensional consolidation", Journal of Applied Physics, **12**, pp.155-164.

[14] Stoker, J. J. 1957. Water waves, Inter science Publishers, Inc., New York.

[15] Zen, K. and Yamazaki, H. 1990. "Mechanism of wave-induced liquefaction and densification in seabed", Soils and Foundations, **31**, pp.161-179.